ACS Chemical Neuroscience

Letter

pubs.acs.org/acschemicalneuroscience

Synthesis and in Vitro Evaluation of a Biotinylated Dextran-Derived Probe for Molecular Imaging

Anurag Mishra,*[,†,∥] Rajendra Joshi,[‡,∥] Jörn Engelmann,[‡] and Nikos K. Logothetis[†,§]

[†]Department for Physiology of Cognitive Processes and [‡]High-Field Magnetic Resonance, Max-Planck Institute for Biological Cybernetics, Spemannstrasse 38, 72076 Tübingen, Germany

[§]Imaging Science and Biomedical Engineering, University of Manchester, Manchester M13 9PL, England

Supporting Information

ABSTRACT: Herein we report the design, synthesis, and in vitro evaluation of a gadolinium-containing biotinylated dextran-derived molecular imaging probe as a prospective neuroanatomical tracer by means of magnetic resonance imaging (MRI). The probe was effectively taken up by cultured differentiated murine neuroblastoma cells and significantly enhanced the contrast in T_1- and T_2-weighted MR images of labeled cells under physiological conditions. A significant longitudinal relaxation rate enhancement in the presence of avidin was observed allowing the verification of the results in the end of noninvasive longitudinal MRI connectivity studies by post-mortem histology. The in vitro results indicate that the probe has the potential to be used in vivo to identify the organization of global neuronal networks in the brain with MRI.

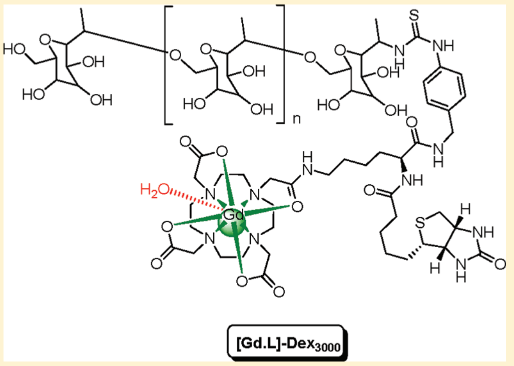

KEYWORDS: *Gadolinium, dextran amine, biotin, imaging probes, magnetic resonance imaging*

It is now widely accepted that the organizational and functional complexity of the brain can be better examined if the knowledge from various scientific fields is employed and combined. In order to study brain organization, it is important to uncover both the anatomical connectivity between different regions as well as to understand the functional mechanisms underlying brain coding in more detail.[1] Currently, the field of neuroscience has been revolutionized by the expansion of neuronal tract-tracing and cell tagging procedures which provide the prospect to identify the organization of global neuronal networks in the brain. Tract-tracing techniques are extremely helpful for revealing valuable information on afferent and efferent connectivity of neuronal networks between various regions in the brain. These techniques are facilitated by the use of a wide variety of neuroanatomical tracers which are generally classified in retrograde and anterograde categories.[2,3]

Thus far, several classical neuroanatomical markers (such as dextran derivatives, biocytin, cholera-toxin subunit-B (CTB), etc.) have been developed which contributed in divulging valuable descriptions of neuronal connectivity in the brain.[4−6] These conventional tracers require in vivo injection in the brain. However, after a specific survival time the studied animal has to be euthanized and employment of *invasive* neurohistochemical techniques involve in vitro tissue processing for data analysis. Therefore, it is highly important to look for alternative methods that can be used in *noninvasive* and longitudinal in vivo studies of brain connectivity.

Magnetic resonance imaging (MRI) is a powerful *noninvasive* medical diagnostic tool that offers high spatial and temporal resolution of in vivo brain structure. Manganese-enhanced MRI (MEMRI) represents the first effort in the direction of longitudinally studying neuronal connectivity in vivo by means of MRI.[7−10] Mn^{2+} is transported anterogradely in the axon and has been widely used in many animal models. However, the technique presents several drawbacks that can challenge its applicability, the most important being the toxicity because of the high tissue concentration of free Mn^{2+} that is required for a sufficient contrast enhancement in the MR images.[11−13]

Recently, as an alternative approach, we have introduced nontoxic modified biocytin (low molecular weight) based MR neuroanatomical tracers.[6,14,15] These MR tracers have potential applications in both revealing neuronal connections in vivo by means of MRI as well as investigating the histology of post-mortem tissue in the same experimental animal model.[6] We have shown excellent short-term neuronal projections by MRI which were confirmed by histological methods.[14] In another report by Wu et al., the conventional high molecular weight neuroanatomical tracer CTB was conjugated with a gadolinium (Gd^{3+}) chelate and used for visualization by MRI.[16]

In this work, we have chosen biotinylated dextran amines (BDAs) as a model molecule. BDAs are hydrophilic polysaccharides with good water solubility and low toxicity. They are also widely employed to trace neuronal projections

Received: November 9, 2011
Accepted: January 16, 2012
Published: January 16, 2012

Scheme 1[a]

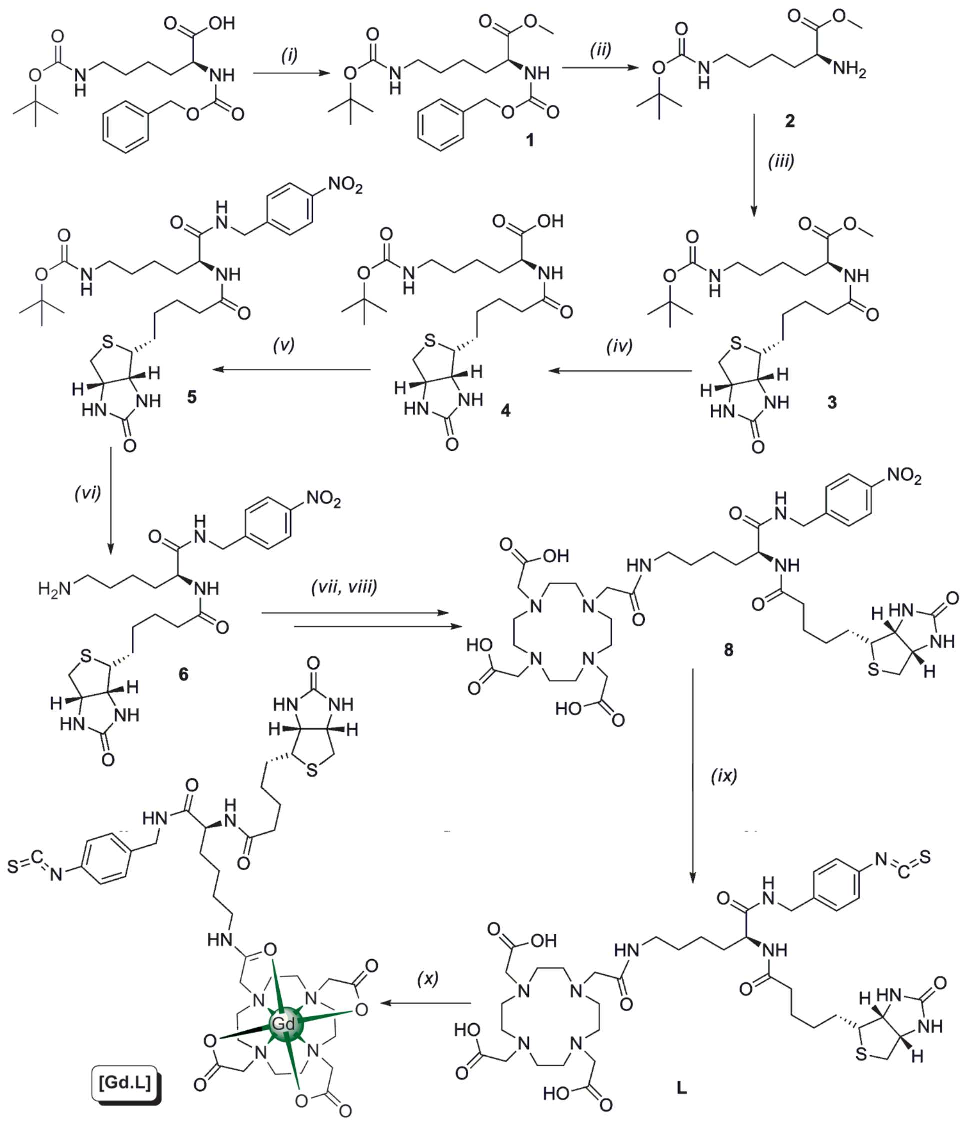

[a]Reagents and conditions: (i) MeOH, NMM, EDC, HOBt, (anhydrous) DMF; (ii) Pd−C (10%), H_2, MeOH, 50 psi; (iii) D-biotin, NMM, EDC,HOBt, (anhydrous) DMF; (iv) LiOH, THF;MeOH;water (3:2:1); (v) p-nitrobenzylamine, NMM, EDC, HOBt, (anhydrous) DMF; (vi) TFA/CH_2Cl_2 (1:10); (vii) tris-*tert*-butyl-DOTA, NMM, EDC, HOBt, (anhydrous) DMF; (viii) neat TFA; (ix) (1) Pd−C (10%), H_2, MeOH, 50 psi; (2) thiophosgene, CCl_4, H_2O, pH 8−8.5; (x) $GdCl_3{\cdot}6H_2O$, H_2O, pH 6.5.

anterogradely or retrogradely by optical techniques. They are biologically inert due to poly-(α-D-1,6-glucose) linkages, which render them resistant to cleavage by most endogenous cellular glycosidases.[17,18] Thus, BDAs are particularly useful for long-term neuronal projections (up to 2 weeks).

Herewith, we report the design, synthesis and in vitro evaluation of a biotinylated Dextran (MW 3000) conjugated MR imaging probe ([**Gd.L**]-**Dex**$_{3000}$). We designed a multipurpose MR precursor [**Gd.L**] to be connected to dextran amine via preloading approach. This macrocyclic MR precursor consists of biotin on the *α-amino* group of a lysine linker (for visualization by immunohistochemical methods), a Gd^{3+} caged organic macrocyclic moiety [**Gd-DOTA**] on the *ε-amine* (as MR reporter), and isothiocyanate benzylamine on the *carboxylic group* of lysine to connect with free amine of Dextran$_{3000}$. The low molecular weight Dextran$_{3000}$ was used because it offers several advantages in comparison to higher molecular weight Dextrans (e.g., with MW 10 000, also used as neuronal tracer) like faster axonal diffusion and greater access to peripheral cell processes.[17,18]

The synthesis of [**Gd.L**] was performed in nine steps prior to complexation with $GdCl_3{\cdot}6H_2O$ (Scheme 1). Starting with 6-(*tert*-butoxycarbonylamino)-2-(5-(2-oxo-hexahydro-1H-thieno-[3,4-d]imidazol-4-yl)pentanamido)hexanoic acid esterification with MeOH [EDC/HOBt/NMM] in DMF to get methyl ester **1**, the corresponding amine **2** was obtained by hydrogenation over Pd−C as the catalyst (H_2/MeOH, 20 °C). The primary amine of **2** was coupled with the acid form of D-biotin [EDC/HOBt/NMM] in DMF to get biotinylated lysine **3** in 68% yield, and the monoacid **4** was obtained by selective deprotection of the methyl group with LiOH. **4** was further coupled with *p*-nitrobenzylamine [EDC/HOBt/NMM] in DMF to get nitro-biotinylated adduct **5**, which was further treated with mild acid, cleaving the Boc group to afford the amine **6**. The macrocycle intermediate tris-*tert*-butyl-DOTA was obtained in two steps by stepwise alkylation of tris-*tert*-

Scheme 2[a]

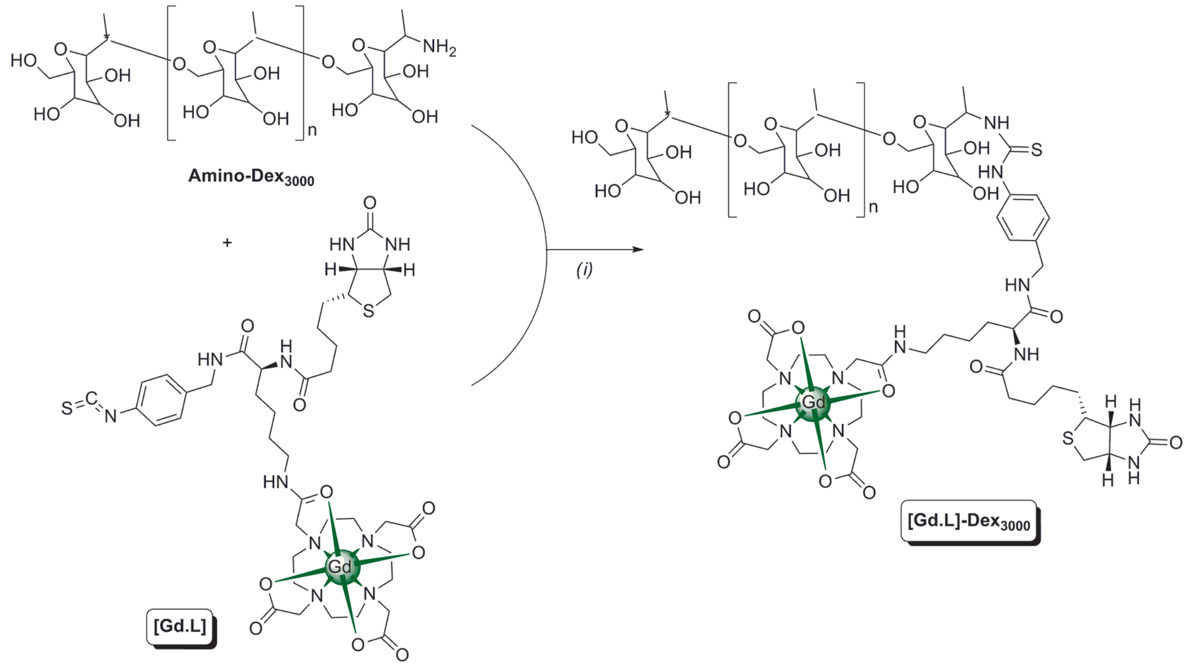

[a]Reagent and condition: (i) H_2O, pH 8.5.

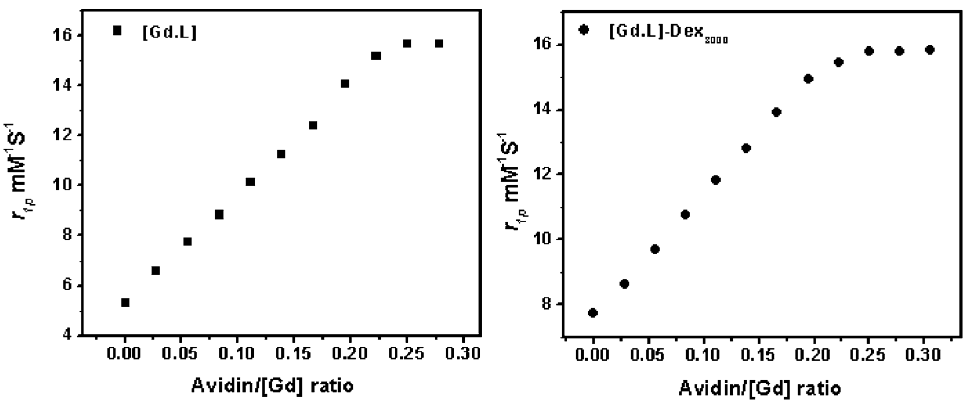

Figure 1. Longitudinal proton relaxivity (r_{1p}) variation under the addition of avidin for an aqueous solution containing [**Gd.L**] and [**Gd.L**]-**Dex**$_{3000}$ (37 °C, 60 MHz, pH 7.4, PBS, 0.27 mM [**Gd.L**] and 0.20 mM [**Gd.L**]-**Dex**$_{3000}$).

butyl-DO3A with benzylbromoacetate in MeCN and following deprotection of benzyl group produced the desired acid derivative in high yield.[19] Thus, tris-*tert*-butyl ester **7** was synthesized by coupling of amine **6** and acid of tris-*tert*-butyl-DOTA [EDC/HOBt/NMM] in anhydrous DMF. The formation of compound **7** was confirmed by ESI-MS and purified by classical column chromatography. Since **7** is a very polar protected ligand, its purification from the crude mixture via silica/alumina columns gave a poor yield. The deprotection of *tert*-butyl groups with TFA on **7** gave the nitro triacetic acid ligand **8** which was purified by RP-HPLC. Isothiocyanate triacetic acid ligand **L** was synthesized in two steps by reducing nitro group of **8** and converting aryl-amine in isothiocyanate by using thiophosgene at pH 8. Macrocyclic precursors **8** and **L** were purified by RP-HPLC and **L** was loaded with Gd^{3+} using $GdCl_3 \cdot 6H_2O$ in water at pH 6.5 to get [**Gd.L**].

The final MR tracer [**Gd.L**]-**Dex**$_{3000}$ was obtained in a one pot conjugation by mixing [**Gd.L**] and Dextran amine in water at pH 8.5. The excess [**Gd.L**] was removed by using Omega 3K PES ultrafiltration membrane with cutoff 3000 Da, and after dialysis solution was lyophilized to obtain off-white solid (Scheme 2). The product formation was confirmed by infrared (IR) spectroscopy. The IR spectra of thiourea of [**Gd.L**]-**Dex**$_{3000}$ show a corresponding band at 1474 cm^{-1}. This band is attributed to the antisymmetric (NCN) stretching of the thiourea. Another IR band at 1413 cm^{-1} was also observed and according to literature this band can be assigned to the C═S vibration.[20] The analytical purity of complex was determined by reverse phase HPLC. The final concentrations of Gd^{3+} complexes ([**Gd.L**] and [**Gd.L**]-**Dex3000**) were determined by inductively coupled plasma optical emission spectrophotometry (ICP-OES).

The proton longitudinal relaxivity (r_{1p}) of the monoaqua MR contrast agents (CAs; [**Gd.L**] and [**Gd.L**]-**Dex**$_{3000}$) at 1.4 T (60 MHz) [phosphate buffered saline (PBS), 7.4 pH, 37 °C] were 5.29 and 7.73 mM^{-1} s^{-1}, respectively. These relaxivities were higher as compared to those of reported [**Gd-DOTA**] derivatives in such physiological solutions and at ambient temperature.[21] This can be explained by the high molecular volume and a significant second-sphere contribution.[22]

It is well-known that BDAs[4] have a high affinity to tetrameric avidin and can be visualized by light microscopy in post-mortem tissues using avidin-conjugated markers. Numerous applications of biotin−avidin interactions have been found attractive in medical diagnostics, biomolecule detection, immunoassays, and nanoscience.[23−25] To explore the binding behavior of the two CAs to avidin which is an important characteristics for the histological detection, we performed in vitro MRI experiments at 1.4T (60 MHz) [PBS, 7.4 pH, 37 °C] with increasing concentrations of avidin proportional to constant concentrations of CAs (0.27 mM [**Gd.L**] and 0.20 mM [**Gd.L**]-**Dex$_{3000}$**) and measured r_{1p}. Expectedly, the linear enhancement in r_{1p} [up to 196% (5.3 → 15.7 mM^{-1} s^{-1}) in [**Gd.L**] and 104% (7.7 → 15.8 mM^{-1} s^{-1}) in [**Gd.L**]-**Dex$_{3000}$**] were observed upon binding to avidin (Figure 1). The observed increase in r_{1p} upon binding to avidin is in agreement with the Solomon−Bloembergen−Morgan theory which predicts that at moderate magnetic fields (≤128 MHz) r_{1p} changes with the inverse of molecular rotational correlation time (τ_R) whereby an increase in relaxivity is expected upon binding of the contrast agent to a large molecule as avidin.[26] This trend was already reported in the literature for fast tumbling low molecular weight Gd^{3+}-chelates.[27,28] A saturation in relaxivities was observed at an approximate ratio of 4:1 for the [**Gd.L**]/[**Gd.L**]-**Dex$_{3000}$:avidin** adducts (Figure 1), which is consistent with the tetrameric nature of avidin.[29] The effective binding to avidin and the 4:1 stoichiometry of the [**Gd.L**]/[**Gd.L**]-**Dex$_{3000}$:avidin** complexes indicates that [**Gd.L**] and [**Gd.L**]-**Dex$_{3000}$** could be easily visualized by interaction with avidin via immunohistochemical methods.

Both [**Gd.L**] and [**Gd.L**]-**Dex$_{3000}$** were now tested in vitro for acute toxicity, cellular uptake, and the ability to enhance contrast in T_1-weighted MR images. For this purpose, murine N18 neuroblastoma cells were used as cellular model. Stepwise serum reduction to 1.25% was used to differentiate the cells and to induce neuronal metabolic and morphologic features in these tumor cells.[30] The growth rate slowed down and cells started to show a neuronal morphology with a network of neurite-like cellular processes which were completely absent at 10% FBS (data not shown).

All further cell incubations were performed in HBSS/10 mM HEPES buffer for 5 h. During this incubation period, no significant influence on the metabolic activity of differentiated N18 cells (as a measure of cell viability) was detected at concentrations below 50 μM for both [**Gd.L**] and [**Gd.L**]-**Dex$_{3000}$** (Figure S1, Supporting Information).

Thus, differentiated N18 cells were labeled with [**Gd.L**] and [**Gd.L**]-**Dex$_{3000}$** at 50 and 40 μM, respectively, to evaluate their ability to enhance contrast in MR images. After the labeling period, cells were extensively washed to remove all unbound extracellular CA. A constant number of labeled cells were transferred to Eppendorf tubes, and the cells were allowed to settle down prior to the MR measurements. T_1-weighted images were taken and the values of longitudinal (T_1) relaxation times were measured in an axial slice of cell pellets at 123 MHz (3T) and room temperature. Figure 2 displays representative T_1-weighted images and the analysis of the corresponding signal intensities of such cell phantoms. A clear and highly significant contrast enhancement was detectable for cells labeled with [**Gd.L**]-**Dex$_{3000}$** compared to unlabeled control cells. When the apparent cellular relaxation rates $R_{1,cell}$ and $R_{2,cell}$ are determined in axial slices through the cell pellet, the contrast enhancing ability of [**Gd.L**]-**Dex$_{3000}$** in cells was confirmed whereas [**Gd.L**] could not significantly increase both relaxation rates (Figure 3). These results indicating that the Dextran-conjugate is sufficiently taken up by neuronal cells to alter significantly the signal intensity in T_1- and T_2-weighted MR images.

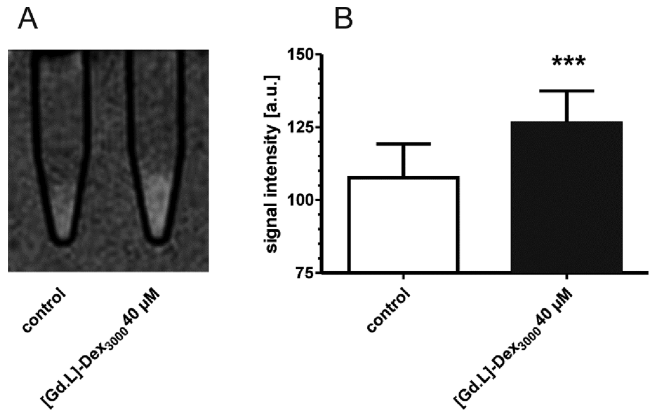

Figure 2. T_1-weigted MR images of differentiated N18 neuroblastoma cells labeled with [**Gd.L**]-**Dex$_{3000}$** (A) and analysis of the corresponding signal intensities (B). Cells were incubated without or with 40 μM [**Gd.L**]-**Dex$_{3000}$** for 5 h in HBSS/10 mM HEPES. Cells were washed, trypsinized, and resuspended in fresh culture medium (without CA) at a cell density of 1 × 10^7 cells/500 μL and transferred into 0.5 mL tubes. Cells were allowed to settle prior to MR experiments for imaging and determination of T_1 values in an axial slice through the cell pellet. Parameters for MRI are given in the Methods part. The bar graphs resulted from the pixelwise evaluation of signal intensity in the corresponding images. Values represent mean ± SD (n = 298); ***, $p > 0.001$, significantly different from control (unpaired Student's t-test).

In summary, [**Gd.L**]-**Dex$_{3000}$** is a promising candidate as imaging probe that could be used to charting longitudinal in vivo connectivities of neuronal networks in the brain by the use of MRI and histological methods. We have presented the design, synthesis, and in vitro evaluation of a new generation of Gd-containing biotinylated Dextran-derived MR tracers. The imaging probe exhibits a significant longitudinal relaxation rate enhancement in the presence of avidin. [**Gd.L**]-**Dex$_{3000}$** was effectively taken up by cultured murine neuroblastoma cells and was significantly enhancing the contrast in T_1- and T_2-weighted MR images without being toxic under these experimental conditions. The results indicate that the probe has the potential to be used in vivo to visualize the connectivity of neuronal networks by means of MR imaging. The binding of [**Gd.L**]-**Dex$_{3000}$** to avidin with a 4:1 binding stoichiometry permits to compare or verify the MR results by neurohistochemical techniques in the same animal model in the end of longitudinal studies. However, the full potential of this compound has to be shown in future in vivo experiments. Overall, the CA we report here represents a new platform for the development of multimodal molecular imaging tools of interest for neuroscience.

■ METHODS

General. The general chemistry, experimental information, syntheses, and characterization of ligands and complexes are supplied in the Supporting Information.

In Vitro Cell Studies of [Gd.L] and [Gd.L]-Dex$_{3000}$. *Cell Culture.* N18 mouse neuroblastoma cells were cultured as a monolayer

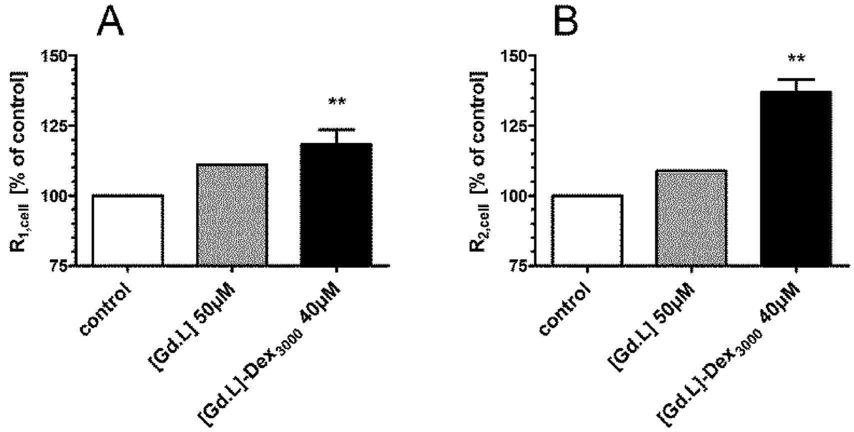

Figure 3. Cellular relaxation rates $R_{1,cell}$ (A) and $R_{2,cell}$ (B) after incubation of differentiated N18 neuroblastoma cells with [**Gd.L**] and [**Gd.L**]-**Dex**$_{3000}$. Cells were incubated without or with 50 μM [**Gd.L**] or 40 μM [**Gd.L**]-**Dex**$_{3000}$ for 5 h in HBSS/10 mM HEPES. Further experimental details as described in Figure 2 and Methods. Data represents mean ± SEM; **, $p < 0.01$ significantly different from control (ANOVA, Dunnett's multiple comparison test).

at 37 °C with 5% CO_2 in antibiotic-free Dulbecco's modified Eagle's medium (DMEM) supplemented with 10% fetal bovine serum (FBS) and 4 mM L-glutamine (all purchased from Biochrom AG, Germany). Cells were passaged by trypsinization with trypsin/EDTA 0.05/0.02% (w/v) in PBS for 5 min every second to third day. In order to induce a neuronal phenotype, the FBS content was reduced stepwise to 1.25% prior to the experiments.

Cytotoxicity of [Gd-L] and [Gd.L]-Dex$_{3000}$. Differentiated N18 cells were inoculated into 96-well plates and treated 48 h later with 0.1−500 μM [**Gd.L**] or [**Gd.L**]-**Dex**$_{3000}$ in HBSS/10 mM HEPES for an additional 5 h.

The metabolic activity as marker for cell viability was determined by XTT-based colorimetric assay. Briefly, medium was removed and cells were further incubated for 30 min in DMEM (without phenol red and CAs) containing XTT (0.25 mM) and PMS (0.5 μM). Cells were thoroughly shaken to dissolve the formed water-soluble formazan dye and the absorbance of the solution was measured at 450 nm and with reference wavelength at 690 nm in a multiplate reader. The measured metabolic activity was expressed as percent of control (cells incubated in a similar way without CA).

MRI on [Gd.L]-Labeled Cells and [Gd.L]-Dex$_{3000}$-Labeled Cells. For MR imaging, serum deprived N18 cells were grown in 175 mL tissue culture flasks for 3−4 days in complete culture medium. Afterward, cells were labeled with 50 μM [**Gd.L**] or 40 μM [**Gd.L**]-**Dex**$_{3000}$ in HBSS/10 mM HEPES for an additional 5 h. Cells similarly incubated in the absence of CA served as control. Cells were washed twice with HBSS and once with PBS (without Ca^{2+} and Mg^{2+}) followed by trypsinization. Subsequently, cells were counted (cell viability was assessed by trypan blue staining), centrifuged, and resuspended in complete culture medium at a cell density of 1×10^7 cells/500 μL and then transferred to 0.625 mL Eppendorf tubes. Before performing MR measurements, cells were allowed to settle in the tubes. Cell pellets were imaged at room temperature (~21 °C) with a clinical 3 T (123 MHz) human MR scanner (MAGNETOM Tim Trio, Siemens Healthcare, Germany), using a 12-channel RF head coil and slice selective measurements from a slice with a thickness of 1 mm positioned through the cell pellet. Relaxation times T_1 were measured using an inversion−recovery sequence, with an adiabatic inversion pulse followed by a turbo-spin−echo readout. Numbers of MR images acquired were in the range 10−15, with the time between inversion and readout varying from 23 to 3000 ms. With a repetition time of 10 s, 15 echoes were acquired per scan and averaged six times. For T_2, a homewritten spin−echo sequence was used with echo times varying from 18 to 1000 ms in about 10 steps and a repetition time of 8 s. Diffusion sensitivity was reduced by minimizing the crusher gradients surrounding the refocusing pulse. All experiments scanned 256^2 voxels in a field-of-view of 110 mm in both directions resulting in a voxel volume of $0.43 \times 0.43 \times 1$ mm^3.

Data analysis was performed by fitting of relaxation curves with self-written routines under MATLAB 7.1 R14 (The Mathworks Inc., United States). The series of T_1 and T_2 relaxation data were fitted to the following equations:

T_1 series with varying $t = T_I$:

$$S = S_0(1 - \exp(-t/T_1)) + S_{(T_I=0)} \exp(-t/T_1)$$

T_2 series with varying $t = TE$: $\quad S = S_0 \exp(-t/T_2)$

Nonlinear least-squares fitting of three parameters S_0, $S_{(T_I=0)}$, and T_1/T_2 was done for manually selected regions of interest with the Trust-Region Reflective Newton algorithm implemented in MATLAB. The quality of the fit was controlled by visual inspection and by calculating the mean errors and residuals. The obtained T_1/T_2 values of the cell pellet were converted to $R_{1,cell}$ (= $1/T_1$) and $R_{2,cell}$ (= $1/T_2$). These were expressed as percent of control ($R_{1,cell}$/$R_{2,cell}$ of cells incubated under similar conditions in the absence of CA). Evaluation of the signal intensities in the T_1-weighted MR images were performed in ImageJ (http://rsb.info.nih.gov/ij) by defining a circular region of interest (ROI) inside one tube image and measuring the mean signal intensity and standard deviation in the included voxels. Further statistical analyses were performed in GraphPad Prism 5.03 (GraphPad Software, Inc.).

■ ASSOCIATED CONTENT

Ⓢ Supporting Information

Experimental details, synthesis, Figure S1 (viability for 24 h incubation), and ESI-MS and HPLC chromatogram of [Gd.L] and [Gd.L]-Dex$_{3000}$. This material is available free of charge via Internet at http://pubs.acs.org.

■ AUTHOR INFORMATION

Corresponding Author

*Mailing address: Department of Chemistry, Durham University, South Road, Durham DH1 3LE, England. E-mail: anurag.mishra@durham.ac.uk.

Author Contributions

‖These authors contributed equally.

Author Contributions

A.M. conceived the project. A.M. and R.J. performed the chemical synthesis. A.M., R.J., and J.E. did the in vitro characterization of the CA. N.K.L. supported the research. All authors wrote the paper.

Funding

This work was supported by the Max-Planck Society. We thank the EC for a Marie Curie Fellowship, PIEF-GA-2009-237253 (A.M.) and the German Ministry for Education and Research, BMBF, FKZ:01EZ0813 (R.J.).

Notes

The authors declare no competing financial interest.

■ ACKNOWLEDGMENTS

The authors would like to thank Hildegard Schulz for excellent technical assistance.

■ REFERENCES

(1) Kandel, E. R., and Mack, S. (2003) A parallel between radical reductionism in science and in art. *Ann. N.Y. Acad. Sci. 1001*, 272−294.

(2) Weiss, P., and Hiscoe, H. B. (1948) Experiments on the mechanism of nerve growth. *J. Exp. Zool. 107*, 315−195.

(3) Kobbert, C., Apps, R., Bechmann, I., Lanciego, J. L., Mey, J., and Thanos, S. (2000) Current concepts in neuroanatomical tracing. *Prog. Neurobiol. 62*, 327−351.

(4) Lanciego, J. L., and Wouterlood, F. G. (2000) Neuroanatomical tract-tracing methods beyond 2000: what's now and next. *J. Neurosci. Methods 103*, 1−2.

(5) Seltzer, B., and Pandya, D. N. (1978) Afferent cortical connections and architectonics of the superior temporal sulcus and surrounding cortex in the rhesus monkey. *Brain Res. 149*, 1−24.

(6) Mishra, A., Dhingra, K., Schüz, A., Logothetis, N. K., and Canals, S. (2009) Improved Neuronal Tract Tracing with Stable Biocytin-Derived Neuroimaging Agents. *ACS Chem. Neurosci. 1*, 129−138.

(7) Koretsky, A. P., and Silva, A. C. (2004) Manganese-enhanced magnetic resonance imaging (MEMRI). *NMR Biomed. 17*, 527−351.

(8) Saleem, K. S., Pauls, J. M., Augath, M., Trinath, T., Prause, B. A., Hashikawa, T., and Logothetis, N. K. (2002) Magnetic resonance imaging of neuronal connections in the macaque monkey. *Neuron 34*, 685−700.

(9) Van der Linden, A., Verhoye, M., Van Meir, V., Tindemans, I., Eens, M., Absil, P., and Balthazart, J. (2002) In vivo manganese-enhanced magnetic resonance imaging reveals connections and functional properties of the songbird vocal control system. *Neuroscience 112*, 467−474.

(10) Watanabe, T., Frahm, J., and Michaelis, T. (2004) Functional mapping of neural pathways in rodent brain in vivo using manganese-enhanced three-dimensional magnetic resonance imaging. *NMR Biomed. 17*, 554−568.

(11) Eschenko, O., Canals, S., Simanova, I., and Logothetis, N. K. (2010) Behavioral, electrophysiological and histopathological consequences of systemic manganese administration in MEMRI. *Magn. Reson. Imaging 28*, 1165−1174.

(12) Hazell, A. S. (2002) Astrocytes and manganese neurotoxicity. *Neurochem. Int. 41*, 271−277.

(13) Takeda, A. (2003) Manganese action in brain function. *Brain Res. Rev. 41*, 79−87.

(14) Mishra, A., Schüz, A., Engelmann, J., Beyerlein, M., Logothetis, N. K., and Canals, S. (2011) Biocytin-Derived MRI Contrast Agent for Longitudinal Brain Connectivity Studies. *ACS Chem. Neurosci. 2*, 578−587.

(15) Mishra, A., Dhingra, K., Mishra, R., Schüz, A., Engelmann, J., Beyerlein, M., Canals, S., and Logothetis, N. K. (2011) Biocytin-based contrast agents for molecular imaging: an approach to developing new in vivo neuroanatomical tracers for MRI.*Neuroimaging* (Bright, P., Ed.), InTech, Rijeka, Croatia, in press.

(16) Wu, C. W., Vasalatiy, O., Liu, N., Wu, H., Cheal, S., Chen, D. Y., Koretsky, A. P., Griffiths, G. L., Tootell, R. B., and Ungerleider, L. G. (2011) Development of a MR-visible compound for tracing neuroanatomical connections in vivo. *Neuron 70*, 229−243.

(17) Veenman, C. L., Reiner, A., and Honig, M. G. (1992) Biotinylated dextran amine as an anterograde tracer for single- and double-labeling studies. *J. Neurosci. Methods 41*, 239−254.

(18) Reiner, A., Veenman, C. L., Medina, L., Jiao, Y., Del Mar, N., and Honig, M. G. (2000) Pathway tracing using biotinylated dextran amines. *J. Neurosci. Methods 103*, 23−37.

(19) Pope, S. J., Kenwright, A. M., Heath, S. L., and Faulkner, S. (2003) Synthesis and luminescence properties of a kinetically stable dinuclear ytterbium complex with differentiated binding sites. *Chem. Commun.*, 1550−1551.

(20)

(21) Caravan, P., Ellison, J. J., McMurry, T. J., and Lauffer, R. B. (1999) Gadolinium(III) Chelates as MRI Contrast Agents: Structure, Dynamics, and Applications. *Chem. Rev. 99*, 2293−2352.

(22) Botta, M. (2000) Second coordination sphere water molecules and relaxivity of gadolinium(III) complexes: Implications for MRI contrast agents. *Eur. J. Inorg. Chem.*, 399−407.

(23) Weizmann, Y., Patolsky, F., Katz, E., and Willner, I. (2003) Amplified DNA sensing and immunosensing by the rotation of functional magnetic particles. *J. Am. Chem. Soc. 125*, 3452−3454.

(24) Caswell, K. K., Wilson, J. N., Bunz, U. H., and Murphy, C. J. (2003) Preferential end-to-end assembly of gold nanorods by biotin-streptavidin connectors. *J. Am. Chem. Soc. 125*, 13914−13915.

(25) Bickel, U., Yoshikawa, T., and Pardridge, W. M. (2001) Delivery of peptides and proteins through the blood-brain barrier. *Adv. Drug Delivery Rev. 46*, 247−279.

(26) Livramento, J. B., Weidensteiner, C., Prata, M. I., Allegrini, P. R., Geraldes, C. F., Helm, L., Kneuer, R., Merbach, A. E., Santos, A. C., Schmidt, P., and Toth, E. (2006) First in vivo MRI assessment of a self-assembled metallostar compound endowed with a remarkable high field relaxivity. *Contrast Media Mol. Imaging 1*, 30−39.

(27) Rohrer, M., Bauer, H., Mintorovitch, J., Requardt, M., and Weinmann, H. J. (2005) Comparison of magnetic properties of MRI contrast media solutions at different magnetic field strengths. *Invest. Radiol. 40*, 715−724.

(28) Caravan, P., Farrar, C. T., Frullano, L., and Uppal, R. (2009) Influence of molecular parameters and increasing magnetic field strength on relaxivity of gadolinium- and manganese-based T-1 contrast agents. *Contrast Media Mol. Imaging 4*, 89−100.

(29) Wilchek, M., and Bayer, E. A. (1990) Biotin-containing reagents. *Methods Enzymol. 184*, 123−138.

(30) Marchisio, P. C., Weber, K., and Osborn, M. (1979) Identification of multiple microtubule initiating sites in mouse neuroblastoma cells. *Eur. J. Cell Biol. 20*, 45−50.